

## Supplementary Information

### Supplementary Section A

#### Experimental Section:

**Materials synthesis:**  $\text{Na}_2\text{CO}_3$  (Sigma-Aldrich,  $\geq 99.5\%$ ),  $\text{Li}_2\text{CO}_3$  (Sigma-Aldrich,  $\geq 99\%$ ),  $\text{Fe}_2\text{O}_3$  (ThermoFisher-Scientific, 99.9%),  $\text{Mn}_2\text{O}_3$  (Sigma-Aldrich,  $\geq 99\%$ ) and  $\text{MnO}_2$  (Sigma-Aldrich,  $\geq 99\%$ ) were mixed homogeneously in a planetary ball mill, pressed into pellets under a pressure of 15 MPa and subsequently calcined at 850°C for 12 hours (under)  $\text{O}_2$  atmosphere. For example, for NLFM, TM-oxide were taken in stoichiometric ratio of  $\text{Fe}_2\text{O}_3$ :  $\text{Mn}_2\text{O}_3$ :  $\text{MnO}_2 = 0.125$ : 0.2: 0.55.  $\text{Li}_2\text{CO}_3$  and  $\text{Na}_2\text{CO}_3$  were taken each in 10% excess to compensate the loss of Li and Na during prolonged high temperature sintering. The resulting mixture was pelletized and then calcined at 850°C in  $\text{O}_2$  atmosphere for 12 hours. After calcination, the samples were allowed to cool to room temperature and subsequently stored in an Ar-filled glove box ( $\text{H}_2\text{O}$  and  $\text{O}_2$  levels  $< 0.1$  ppm) to prevent air and moisture exposure.

**Electrochemical testing:** For electrode coating, slurry of cathode material, carbon black (C45) and polyvinylidene difluoride in 8:1:1 wt. ratio was prepared in N-methyl-2-pyrrolidone (NMP); casted onto aluminum foil and dried under vacuum (100°C), roll-pressed and cut into 15 mm diameter electrode disks. For CR2032-type coin cell (SS316L, AOT) assembly we used 1 M  $\text{NaPF}_6$  (Sigma-Aldrich, 98%) in propylene carbonate (PC, anhydrous, Sigma-Aldrich, 99.7%) as electrolyte solution and soaked in glass fiber filter (GF/D, Whatman) separator; Na-metal as anode. All electrochemical tests were performed using Biologic battery cycler (BCS-805). Cyclic voltammetry was performed at 0.1 mV/S scan rate for checking redox and reversibility. Galvanostatic charge-discharge cycling was performed at different current rates (at C/10, 1C and 5C rates) and over varying voltage regions for multiple cycles. , For rate studies, slow charge (C/10) and varying discharge rates from C/10 to 5C was used. Galvanostatic intermittent titration technique (GITT) was applied over the entire voltage range of 2.0-4.5 V with a current pulse equivalent to a C/10 rate for 10 minutes, followed by an hour of relaxation. The GITT voltage profiles of NLFM were plotted along with the calculated sodium-ion diffusion coefficient ( $D_{\text{Na}^+}$ ) values. Full cell was fabricated using our cathode and precycled hard carbon anode (lab synthesized from sugar) with above mentioned electrolyte in CR-2032 type coin cells and cycled in the voltage window of 1.2-4.2 V.

#### Details of advanced characterization methods:

**XRD and Ex-situ XRD measurements:** X-ray diffraction (XRD) patterns of NLFM and NLFM1 were recorded at room temperature using a Bruker D8 Advance diffractometer with  $\text{Cu K}\alpha$  radiation ( $\lambda = 1.5406 \text{ \AA}$ ), operating at 40 kV and 40 mA. Rietveld refinements of the collected patterns were carried out using the FullProf software to obtain detailed structural information. For all ex-situ studies, the cathodes were charged/discharged to required state of charge. For this, we use a low current-rate (C/10) to eliminate any kinetic-effects and use a voltage cut off method while also closely monitoring the total charge passed to avoid any discrepancy. Once the required SOC is reached the cell is removed and

quickly disassembled to reduce discrepancies arising out of self-discharge phenomenon. Collected electrodes were thoroughly washed with propylene carbonate (PC) to remove salt impurities and dried under vacuum. During measurements, collected dry electrodes were covered with a thin aluminum foil (10  $\mu\text{m}$  thickness, 99% metal basis, Alfa Aesar) in Ar filled glove box ( $\text{O}_2 < 0.1 \text{ ppm}$ ,  $\text{H}_2\text{O} < 0.1 \text{ ppm}$ ). XRD data were collected at various states of charge and discharge across multiple cycles to monitor changes in lattice parameters during electrochemical cycling.

**Neutron Diffraction:** Multi-Position Sensitive Detector (PSD) based Focusing Crystal Diffractometer (FCD) set up by UGC-DAE Consortium for Scientific Research Mumbai centre at the National Facility for Neutron Beam Research (NFNBR), Dhruva reactor, Mumbai (India) was utilized to carry out Neutron diffraction (ND) study.<sup>S1</sup> The neutron beam of wavelength 1.48 $\text{\AA}$  was used in the experiment. The sample in powder form was placed in vanadium sample holder which was sealed with proper oring to avoid the contact of air. The vanadium sample holder was directly exposed to neutron beam for room temperature neutron diffraction study. The obtained data were analyzed using Rietveld method by using the FullProf program.<sup>S2</sup>

**Field Emission Scanning Electron Microscopy analysis (FE-SEM):** Field emission scanning electron microscopy (FE-SEM) images were collected using a JEOL JSM-7500F microscope.

**Thermogravimetric analysis (TGA):** TGA was carried out by a PerkinElmer TGA 4000 system at the temperature range from 25 $^\circ$ -800 $^\circ\text{C}$  with a heating rate of 10 $^\circ\text{C}/\text{min}$  under  $\text{N}_2$  atmosphere.

**Inductively Coupled Plasma Optical Emission Spectrometry (ICP-OES):** The elemental compositions in the samples were determined by an ICP-OES (PerkinElmer Optima 2100DV) instrument.

**XANES & EXAFS Measurements:** X-ray absorption (XAS) spectroscopy measurements of pristine and cycled electrodes at various states of charge were collected at the P65 beamline of PETRA-III, DESY, Hamburg. Fe and Mn K-edge spectra were recorded at room temperature in transmission mode. Ex-situ electrodes were sealed between Kapton tapes inside an Ar-filled glove box and used directly for measurements. A Si (111) double crystal monochromator was employed, and all data were collected at room temperature. Data processing and analysis were carried out using the Demeter software package, specifically with Athena.

**$^{57}\text{Fe}$  Mössbauer:** Mössbauer spectra of NLFM (pristine) and NLFM (charged 4.5 V) samples were recorded using a Mössbauer spectrometer operated in constant acceleration mode (triangular wave) in transmission geometry at room temperature. The source employed was Co-57 in Rh matrix of strength 50 mCi. The calibration of the velocity scale is done by using an enriched  $\alpha$ - $^{57}\text{Fe}$  metal foil. The isomer shift ( $\delta$ ) values are relative to Fe metal foil ( $\delta = 0.0 \text{ mm/s}$ ).

**SXAS and RIXS:** Soft X-ray XAS measurements were performed at the Veritas RIXS beamline of the MAX IV Laboratory, utilizing a linear vertical (LV) polarized, monochromatized soft X-ray beam. The spectra were collected at the O-K edge (between 520 and 540 eV) in total fluorescence yield (TFY) modes to probe surface and bulk sensitivity, respectively. The samples were mounted under vacuum in a chamber with a base pressure better than  $10^{-8}$  mbar, and spectra were recorded at room temperature. RIXS measurements were conducted using a high-resolution soft X-ray spectrometer based on Rowland circle geometry. The detector was micro channel plate (MCP) based delay line detector (DLD) that

allows for data collection synchronized with electron bunches of the synchrotron. This helps in simultaneous data acquisition and background removal. Here we carried out RIXS energy maps at LV polarization and incident photon energy tuned across the O K-edge (energy range from 528 to 534 eV) to selectively probe the resonant excitation processes. The overall energy resolution (combined beamline and spectrometer) was optimized approximately around 60 meV, measured by fitting the elastic line from a carbon tape with a Gaussian profile. We deliberately settle for a worse resolution since our experimental plans demand high photon flux at the cost of resolution. At this resolution, the vibrational progressions near the elastic line are still very well resolved.

**Computational Details:** First-principles calculations were carried using the projected augmented wave (PAW) method<sup>S3</sup> and the generalized gradient approximation with the Perdew-Burke-Ernzerhof parametrized exchange-correlation functional,<sup>S4</sup> as implemented in the Vienna Ab-initio Simulation Package (VASP).<sup>S5,S6</sup> The DFT+U approach<sup>S7</sup> was adopted to accurately capture the strong correlation effect of localized *3d* electrons in Mn and Fe, using *U* values of 5.0 and 4.9 eV, respectively.<sup>S8</sup> All the structural optimizations were done with the plane-wave cut-off energy of 500 eV and a k-density of  $2\pi \times 0.04 \text{ \AA}^{-1}$  in each direction was applied using the Monkhorst-Pack scheme.<sup>S9</sup> All the calculations (geometry optimization) were spin-polarized and performed until all the forces acting on ions were less than 0.02 eV/Å per atom. To determine the ground state structure initially, a large set of structures with varying Fe ordering configurations was systematically enumerated. The relative energies of these structures were then calculated, and the structure with the lowest energy was identified as the thermodynamically most stable ground state for P2-Na<sub>0.625</sub>Fe<sub>0.125</sub>Mn<sub>0.875</sub>O<sub>2</sub>. Using the consistent arrangement of Fe in the transition metal (TM) layer from the ground state structure, a large set of Li occupation configurations within the TM/AM layer was generated. Finally, the one with the lowest energy was selected as the thermodynamically stable configuration for P2-Na<sub>0.625</sub>Li<sub>0.125</sub>Fe<sub>0.125</sub>Mn<sub>0.125</sub>(III)Mn<sub>0.625</sub>(IV)O<sub>2</sub> (P2-NLFM). A similar approach was followed to determine the Li and Na ordering for the P2-Na<sub>0.79</sub>Li<sub>0.210</sub>Fe<sub>0.125</sub>Mn<sub>0.667</sub>O<sub>2</sub> (containing high Li and Na content). Theoretical modelling of targeted materials was slightly deviated from experimental composition due to computational constraints and complexity to achieving precise stoichiometry. Since the number of Li, Fe, and Mn atoms in a unit cell must be whole numbers, there is a minor discrepancy between the simulated formula and the actual composition. However, this small difference is negligible and can be reasonably ignored. To assess the electronic structure properties in P2-NLFM at various states-of-charges, we carried out spin-polarized DFT calculations using the Heyd-Scuseria-Ernzerhof (HSE06) hybrid functional. A screening parameter ( $\omega$ ) of 0.11 Å<sup>-1</sup> and an exact exchange mixing parameter of 0.25 were applied consistently across all calculations. Structures were visualised using the VESTA software.<sup>S10</sup>

**Ab initio molecular dynamics (AIMD) simulations:** To investigate the ionic diffusion and structural transition, first-principle (*ab initio*) molecular dynamics simulations were carried out for canonical ensemble (NVT) by using a Nose-Hoover thermostat<sup>S11</sup> at 800 K, with a minimal gamma-centered k-mesh. The simulations were conducted for 50 ps with a time step of 1 fs for integrating the equations of motion. The mean square displacement (MSD) of Na<sup>+</sup> and transition metals was computed by

averaging their displacement over time duration  $t$ , where the  $r_i(t)$  represents the displacement of the  $i^{\text{th}}$  mobile ions at time  $t$  and  $t_0$  is the starting time.

$$\text{MSD} = \frac{1}{N} \sum_{i=1}^N \langle [r_i(t + t_0)]^2 - [r_i(t_0)]^2 \rangle \dots (1)$$

The probability density of mobile ions was determined through ensemble averaging over the trajectories.<sup>S12</sup> All the post-processing analysis of AIMD simulation outputs were conducted using Pymatgen and pymatgen-difusion packages.<sup>S13</sup>

**Correlation of ion dynamics:** The van Hove correlation function analysis<sup>S14</sup> was performed to understand the correlations in Na ionic motion. The self-part  $G_s$  of the van Hove correlation function ( $G$ ) are given by

$$G_s(r, t) = \frac{1}{4\pi r^2 N_d} \left\langle \sum_{i=1}^{N_d} \delta(r - |r_i(t_0) - r_i(t + t_0)|) \right\rangle_{t_0}$$

Here, the  $\delta(\cdot)$  represents the one-dimensional Dirac delta function and the angular bracket  $\langle \rangle$  is the ensemble average over the initial time  $t_0$ . The  $r_i(t)$  stands for the position of the  $i^{\text{th}}$  Na-ions at the time  $t$ . The  $N_d$  and  $r$  are the diffusing sodium ions in the unit cell and the radial distance, respectively.

## Supplementary Section B

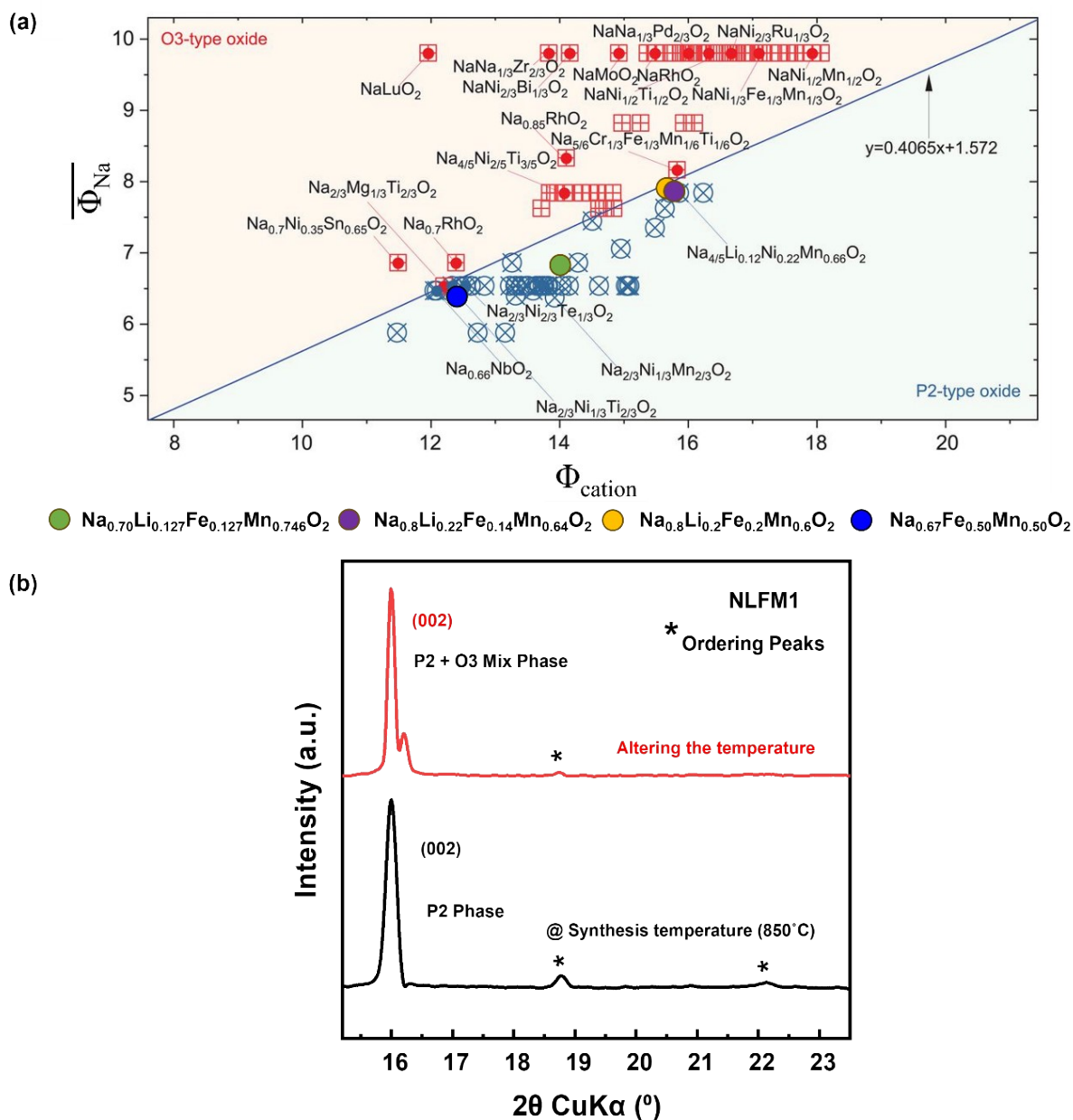


**Figure S1.** (a) Rouxel diagram showing the cationic potential of representative P2 and O3-type Na-ion layered oxides, considering the Na content, oxidation state of transition metals, and TM composition. Our materials are represented with colored dots. [Adopted from Fig. 1B (Ref. 11) and then modified] (b) PXRD comparison of NLFM1 between P2 phase (at synthesis temperature 850°C) and P2 + O3 mix phase (altering the temperature by  $\pm 50^\circ\text{C}$ ).

As NLFM1 has a cationic potential of 15.76, it lies just below the P2-O3 barrier line in the Rouxel diagram. We synthesized NLFM1 via calcination at 850 °C for 12 hours in an O<sub>2</sub> atmosphere. With careful control, we achieved the P2 phase, but slight temperature variations led to a P2/O3 mixed phase.

**Table S1.** Rietveld Refinement Results on the PXRD Pattern of NLFM1.

Space group  $P6_3/mmc$  (No. 194),  $\chi^2 = 3.118$   
 $a = b = 2.8796(1) \text{ \AA}$ ,  $c = 11.1342(0) \text{ \AA}$ ,  $V = 79.95(7) \text{ \AA}^3$

Composition:  $\text{Na}_{0.8}\text{Li}_{0.22}\text{Fe}_{0.14}\text{Mn}_{0.64}\text{O}_2$

Atom	Site	x	Y	z	Occupancy	$B_{\text{iso}}$
Na <sub>f</sub>	2b	0	0	0.25	0.316(2)	2.82(4)
Na <sub>c</sub>	2d	0.33333	0.66667	0.75	0.484(1)	2.82(7)
Li	2a	0	0	0	0.220(4)	0.22(6)
Fe	2a	0	0	0	0.138(2)	0.24(5)
Mn	2a	0	0	0	0.641(2)	0.24(5)
O	4f	0.33333	0.66667	0.09192	1.0000	0.88(5)

Note, NLFM1 has clear Li:TM superstructure ordering peaks in the region  $2\theta$  region  $18^\circ$  to  $31^\circ$ ,  $P6_3/mmc$  space group does not account for this superstructure ordering.

**Table S2a.** Rietveld Refinement Results on the PXRD Pattern of NLFM.

Space group  $P6_3/mmc$  (No. 194),  $\chi^2 = 2.064$ ,  
 $a = b = 2.9017(1) \text{ \AA}$ ,  $c = 11.1295(3) \text{ \AA}$ ,  $V = 81.15(5) \text{ \AA}^3$

Composition:  $\text{Na}_{0.702}\text{Li}_{0.127}\text{Fe}_{0.127}\text{Mn}_{0.746}\text{O}_2$

Atom	Site	X	y	z	Occupancy	$B_{\text{iso}}$
Na <sub>f</sub>	2b	0	0	0.25	0.305(3)	2.79(9)
Na <sub>c</sub>	2d	0.33333	0.66667	0.75	0.397(6)	2.79(9)
Li	2a	0	0	0	0.127(8)	0.34(9)
Fe	2a	0	0	0	0.127(8)	0.42(0)
Mn	2a	0	0	0	0.745(5)	0.22(0)
O	4f	0.33333	0.66667	0.0919	1.0000	0.82(9)

**Table S2b.** Rietveld Refinement Results on the NPD Pattern of NLFM.

Composition:  $\text{Na}_{0.702}\text{Li}_{0.127}\text{Fe}_{0.127}\text{Mn}_{0.746}\text{O}_2$

An impurity phase of 3.06%  $\text{Na}_2\text{CO}_3$  was detected, attributed to exposure to air and moisture during the neutron powder diffraction (NPD) measurement

$P6_3/mmc$ : main phase, $a = b = 2.8732(1) \text{ \AA}$ , $c = 11.1464(8) \text{ \AA}$ , $\alpha = \beta = 90^\circ$ , $\gamma = 120^\circ$ Phase fraction = 96.94, $R_{\text{wp}} = 7.99\%$ , $\chi^2 = 5.58$ .					
Atomic position	x	Y	z	Occupancy	$B_{\text{iso}}$
Na1	0.33333	0.66667	0.75000	0.397(6)	2.446(2)
Na2	0.00000	0.00000	0.25000	0.305(3)	4.119(2)
Mn1	0.00000	0.00000	0.00000	0.745(5)	0.026(9)
Fe	0.00000	0.00000	0.00000	0.127(8)	0.320(3)
Li	0.00000	0.00000	0.00000	0.127(8)	0.028(2)
O1	0.33333	0.66667	0.09195	1.0000	0.045(2)
$\text{Na}_2\text{CO}_3$ : $C2/m$ (No. 12), $a = 8.8895(5) \text{ \AA}$ , $b = 5.2361(4) \text{ \AA}$ , $c = 6.0478(8) \text{ \AA}$ ,					

$\alpha = 90, \beta = 101.31, \gamma = 90, \text{Phase fraction} = 3.06$					
Na1	0.00000	0.01800	0.00000	0.50000	0
Na2	0.00000	0.02200	0.50000	0.50000	0
Na3	0.29944	0.73066	0.83198	1.00000	0
C	0.16400	0.51447	0.27746	1.00000	0
O1	0.11579	0.20982	0.27677	1.00000	0
O2	0.38600	0.46221	0.25456	1.00000	0
O3	0.05881	0.68548	0.21991	1.00000	0

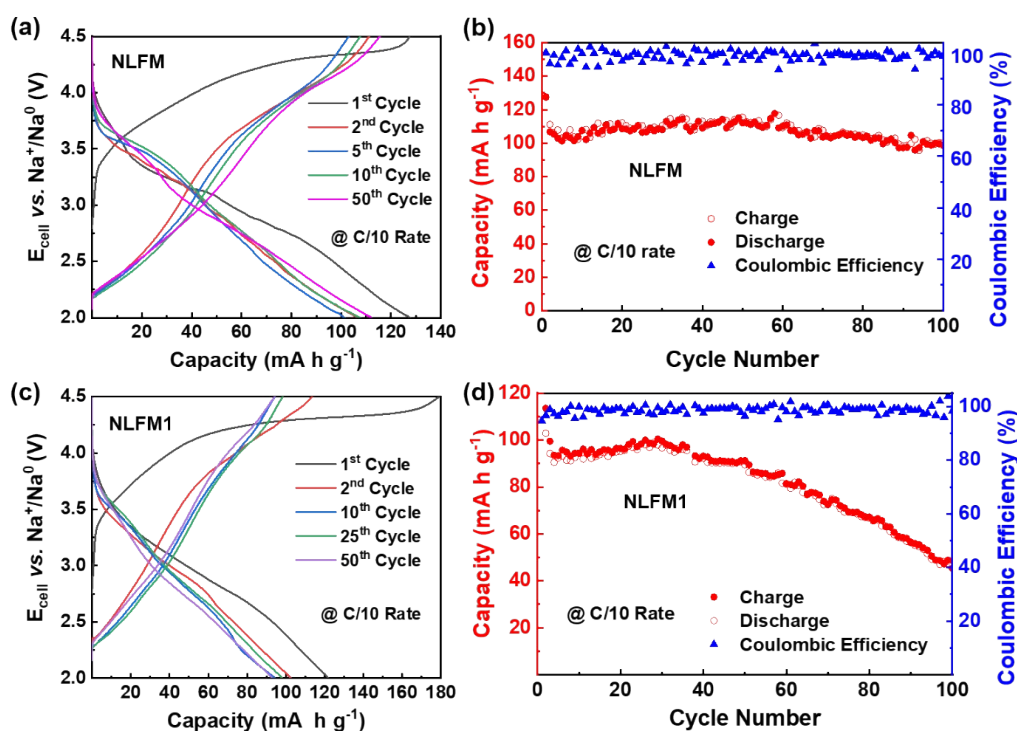


**Figure S2.** Electrochemical characterization in Na half-cells: (a), (c) representative charge/discharge curves at C/10 rate and (b), (d) charge/discharge capacity and Coulombic efficiency as a function of cycle number at C/10 in the voltage range of 2.0–4.5 V of NLFM and NLFM1, respectively.

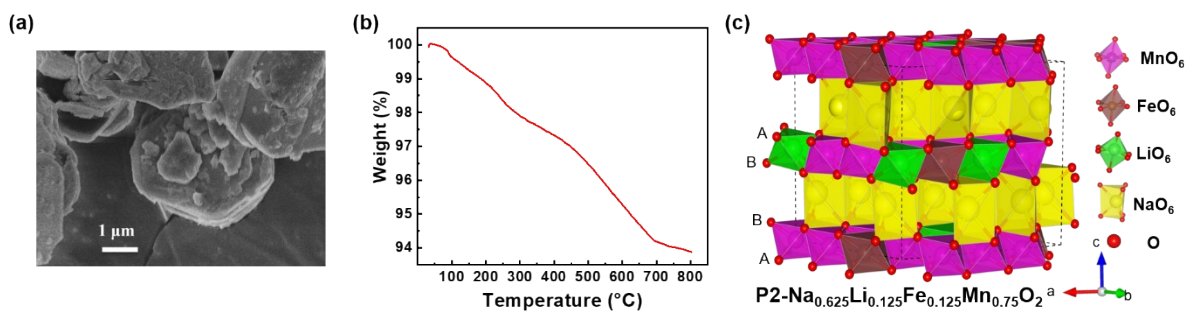


**Figure S3.** (a) FESEM image, (b) TGA data up to 800°C of NLFM and (c) schematic illustration of energetically most stable  $\text{P2-Na}_{0.625}\text{Li}_{0.125}\text{Fe}_{0.125}\text{Mn}_{0.75}\text{O}_2$  (comparable to NLFM) identified among a set

of enumerated structures, where the alkali metal layer consists of trigonal prismatic  $\text{Na}^+$  sandwiched between TM layers of octahedral Fe and Mn partially substituted with Li. Color codes: Mn-O polyhedra: pink, Fe-O polyhedra: brown, Li-O polyhedra: green, Na-O polyhedra: yellow, and O in red.

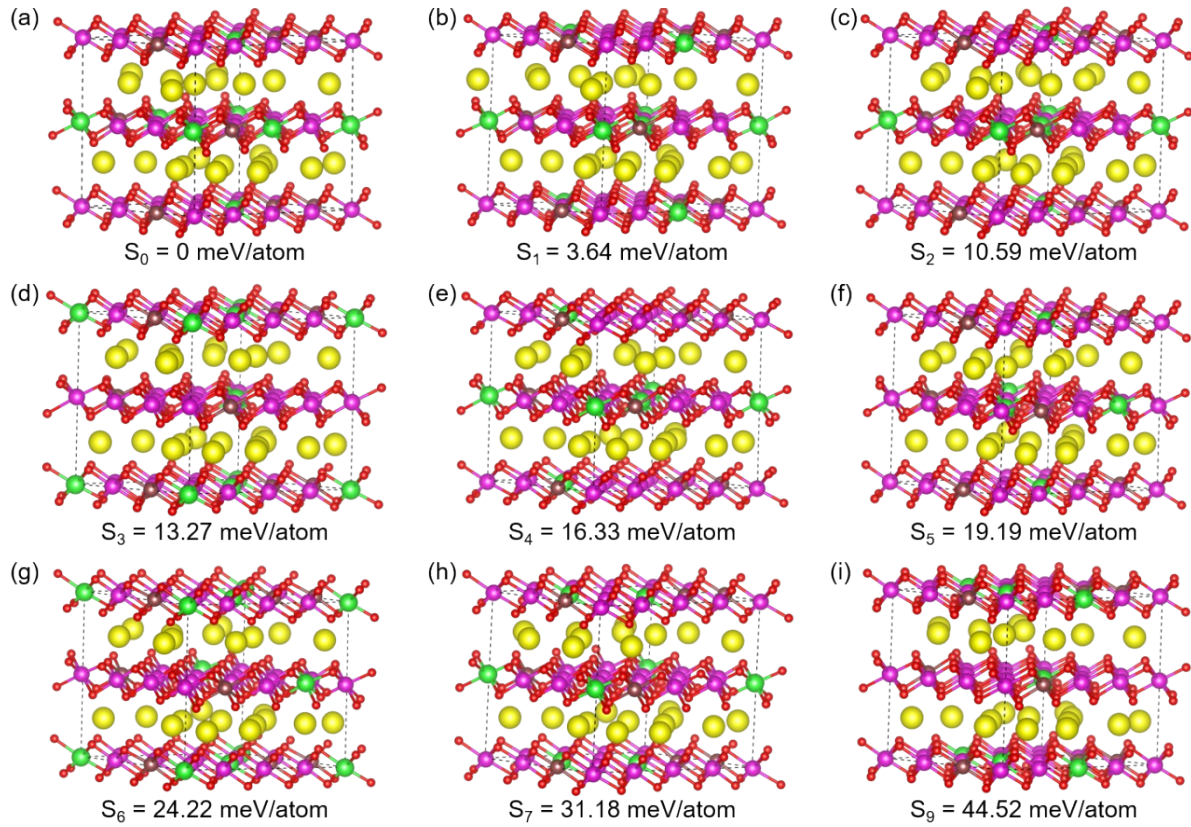


**Figure S4.** Structural illustration of Li ordering in P2  $\text{Na}_{0.625}\text{Li}_{0.125}\text{Fe}_{0.125}\text{Mn}_{0.75}\text{O}_2$  (comparable to NLFM), highlighting  $\text{Li}^+$  ions residing in the transition metal layer, along with their corresponding relative energies ( $E_R$ ) in meV/atom.

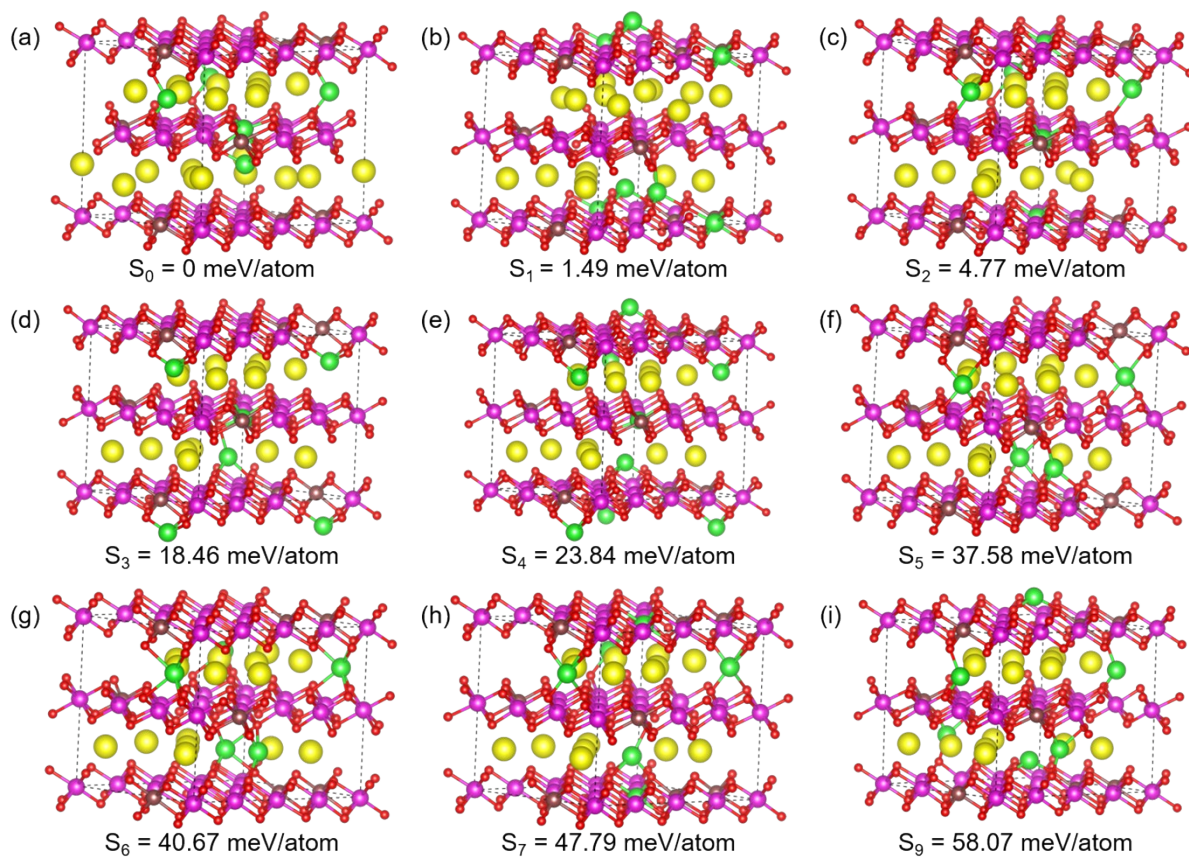


**Figure S5.** Structural illustration of Li ordering in P2  $\text{Na}_{0.625}\text{Li}_{0.125}\text{Fe}_{0.125}\text{Mn}_{0.75}\text{O}_2$  (comparable to NLFM), highlighting  $\text{Li}^+$  ions residing in the Alkali metal layer, along with their corresponding relative energies ( $E_R$ ) in meV/atom. After structural relaxation without any constraints,  $\text{Li}^+$  ions tend to migrate from the AM layer and preferentially occupy vacancies within the transition metal (TM) layer.

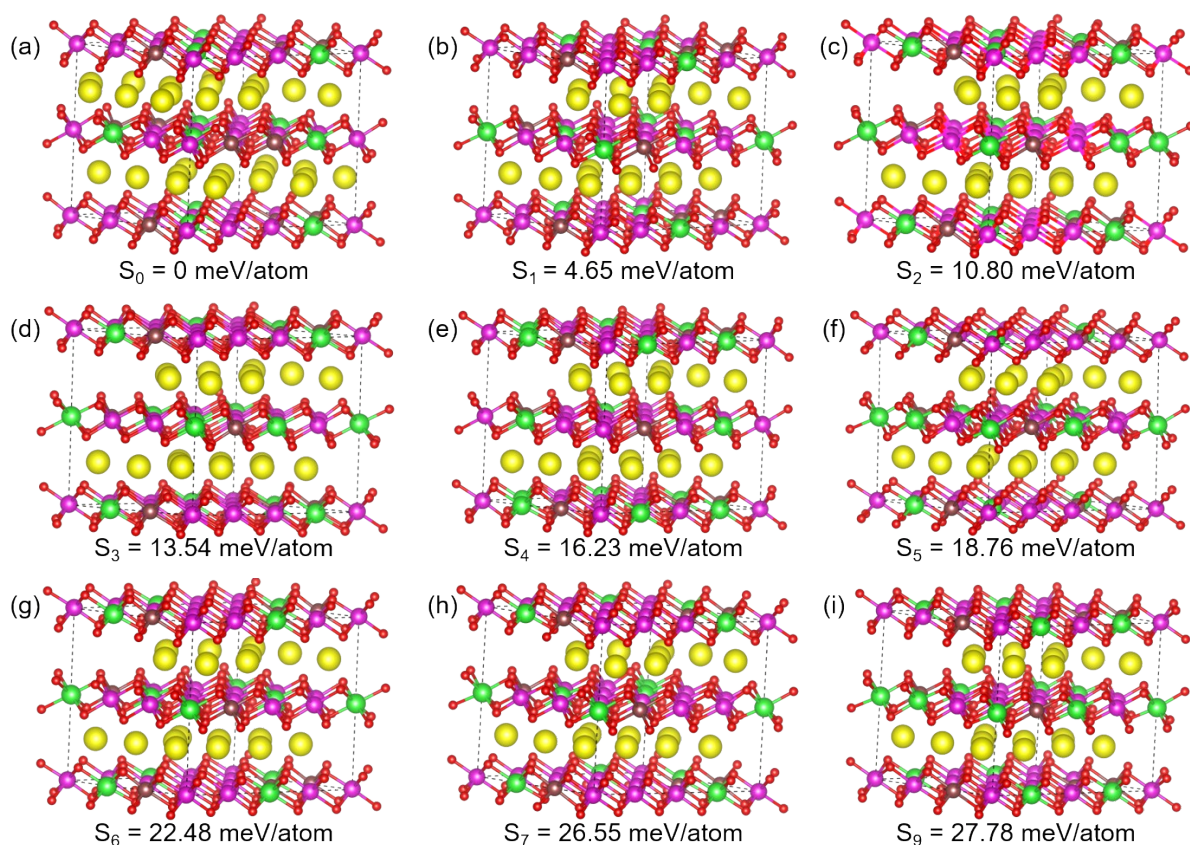


**Figure S6.** Structural illustration of Li and Na ordering in P2  $\text{Na}_{0.79}\text{Li}_{0.210}\text{Fe}_{0.125}\text{Mn}_{0.667}\text{O}_2$  (comparable to NLFM1), depicting their arrangements and corresponding relative energies ( $E_R$ ) in meV/atom.

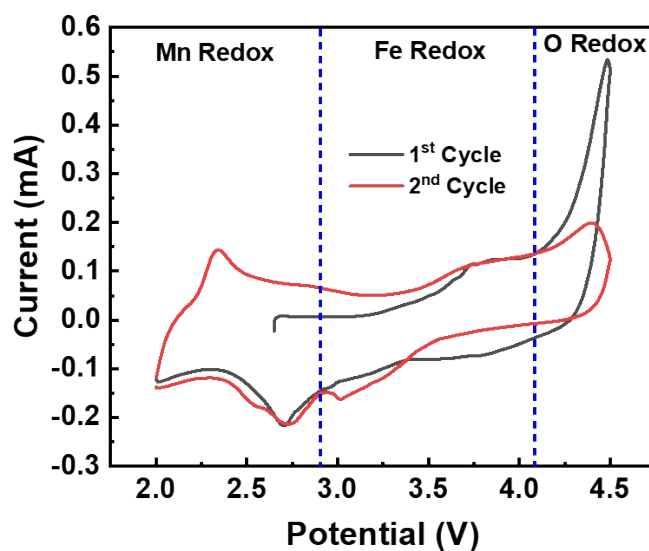


**Figure S7.** Cyclic voltammetry of NLFM at scan rate of 0.1 mV/s.

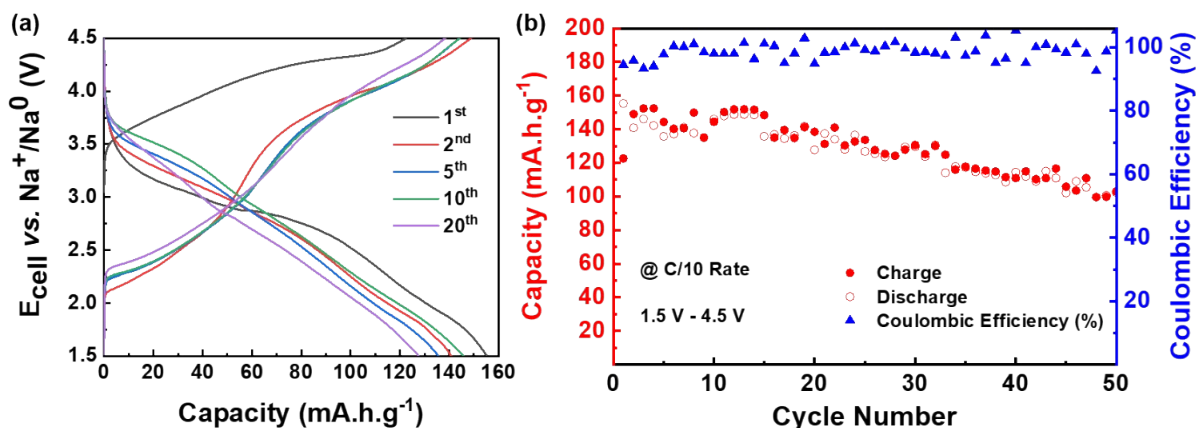


**Figure S8.** (a) Electrochemical characterization of NLFM in Na half-cells: (a) representative charge/discharge curves at C/10 rate, (b) charge/discharge capacity and Coulombic efficiency as a function of cycle number in the voltage range of 1.5–4.5 V.

When discharged to a lower voltage range of 1.5 V (*i.e.*, 1.5V-4.5 V range) NLFM shows first cycle discharge capacity of  $155 \text{ mA h g}^{-1}$  due to  $\text{Mn}^{3+}$  formation. In this voltage range the material shows a poorer capacity retention of only 66% after 50 cycles indicating deleterious effects of cooperative JT distortion kicking in due to presence of higher  $\text{Mn}^{3+}$  content.

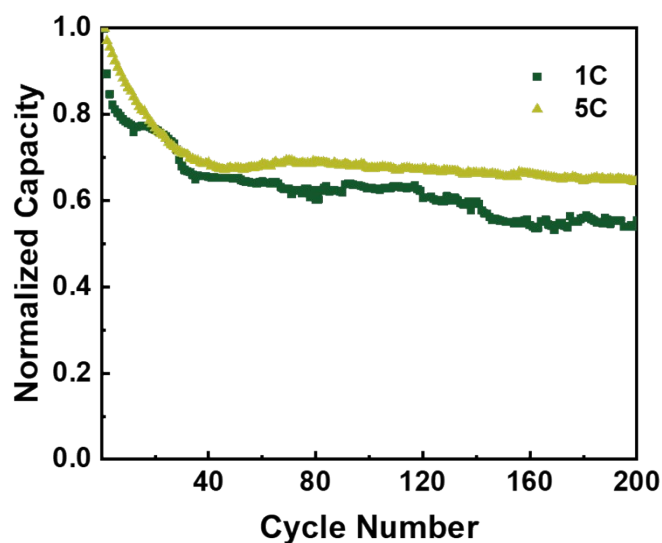


**Figure S9.** Normalized capacity representation of NLFM at charge and discharge at 1C and 5C current rates.

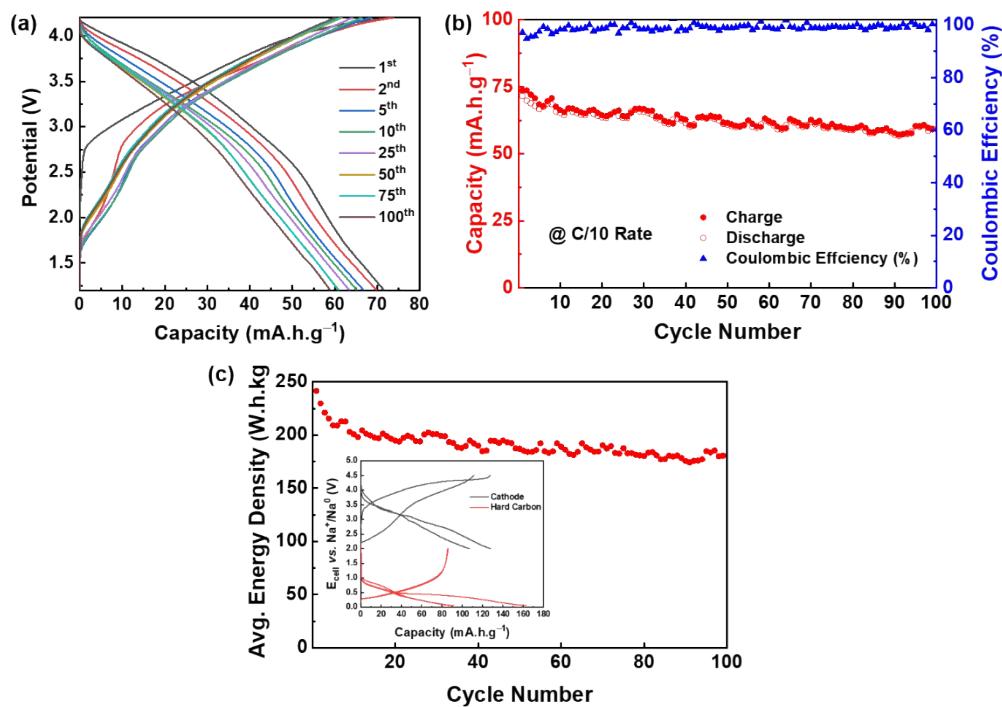


**Figure S10.** For NLFM full cell: (a) Representative charge/discharge curves at C/10 rate, (b) charge/discharge capacity and Coulombic efficiency as a function of cycle number and (c) average energy density retention up to 100 cycles in the voltage range of 1.2–4.2 V (Inset: cathode (NLFM) and anode (hard carbon) capacity comparison).

We have studied the full cell performance of NLFM vs hard carbon anode. The cell delivers a capacity of  $72 \text{ mAh g}^{-1}$  equivalent to energy density of  $238 \text{ Wh/kg}$  energy density retention of  $\sim 83\%$  retention after 100 cycles. It is to be noted that the anode we used delivered a first cycle capacity of only  $162 \text{ mAh g}^{-1}$  in our Na half cells which is almost half of the capacity generally reported for commercial anodes. We therefore conclude that the energy density that we achieve in our full cells is significantly lower than the actual achievable energy density from the cathode material (*i.e.*, when combined with higher quality commercial hard carbon anodes).

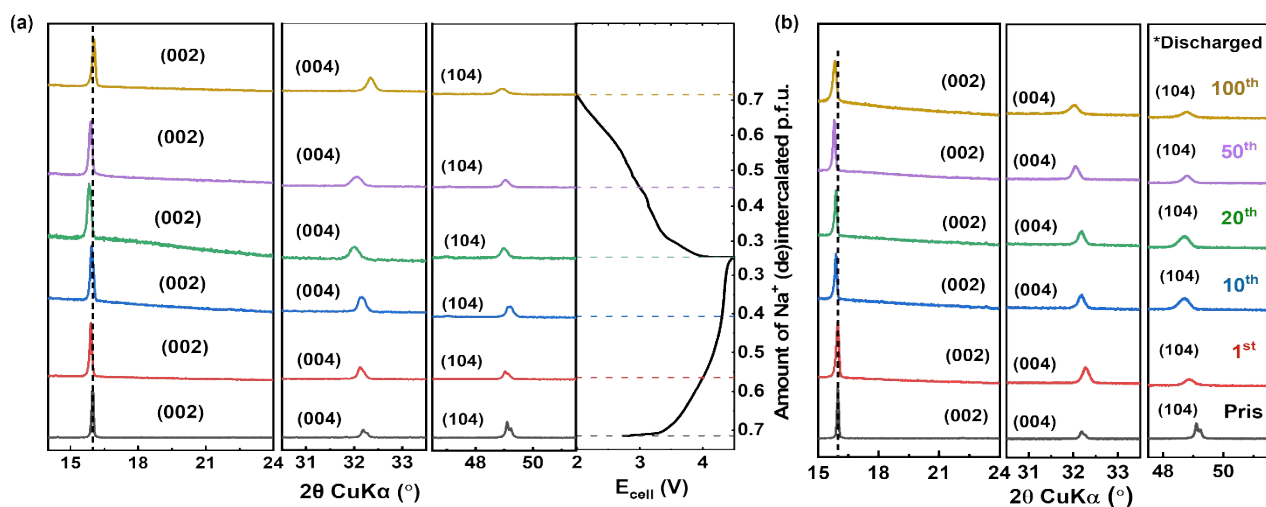


**Figure S11.** (a) Ex situ XRD patterns of P2-NLFM at different states of charge of 1<sup>st</sup> cycle at C/10 rate in the voltage range of 2.0–4.5 V, (b) 1<sup>st</sup> to 100<sup>th</sup> cycle (discharged) ex-situ XRD pattern.

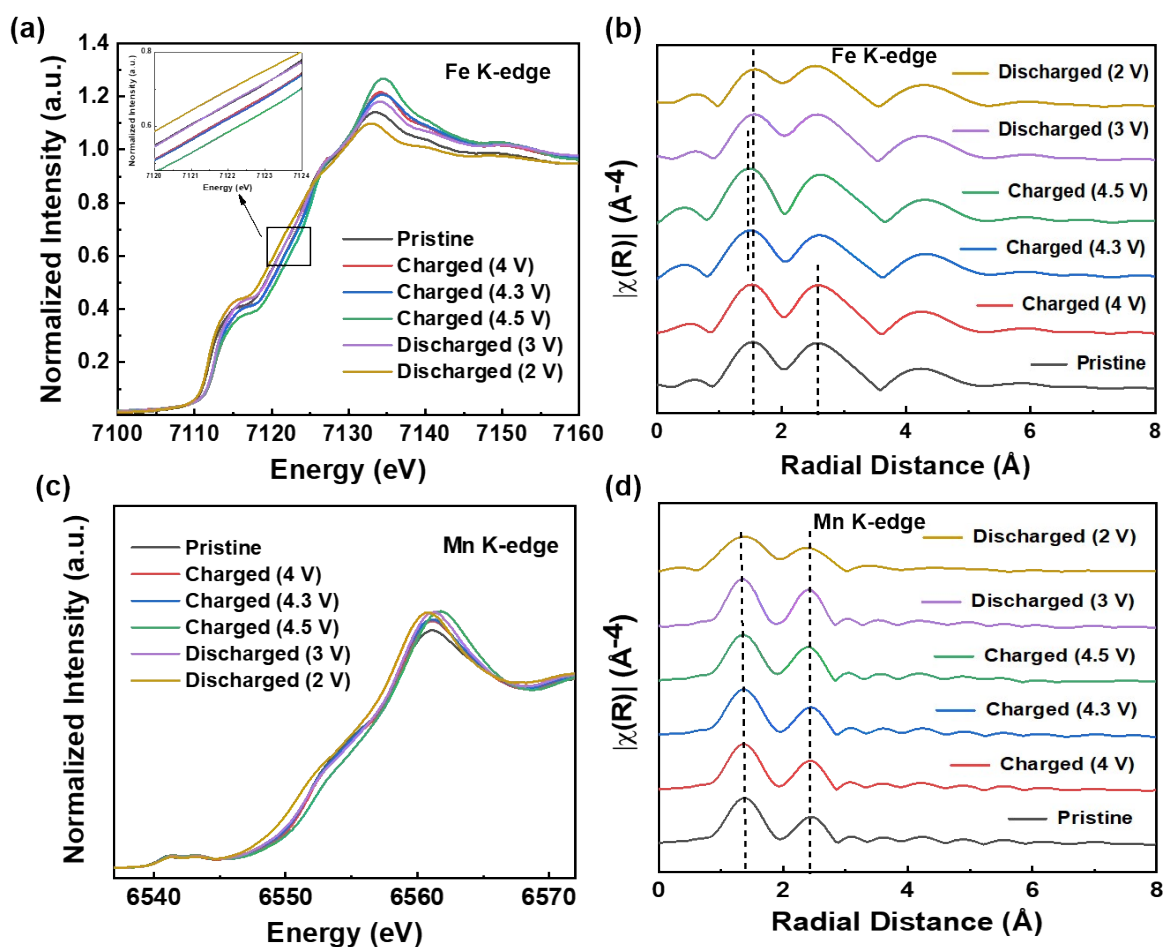


**Figure S12.** (a and c) Normalized ex situ XANES spectra of NLFM collected at different states of charge in 1<sup>st</sup> cycle and (b and d) Corresponding EXAFS spectra collected at Fe and Mn K-edge respectively. During Na deintercalation, the Fe K-edge spectrum changes its edge energy towards higher energy and reverts back on discharge over multiple charge-discharge cycles, suggesting reversible the Fe redox. The decrease in Fe-O distance from 1.53 Å in pristine to 1.46 Å in charged sample corroborates this. The Fe-M distance also shifts slightly, from 2.58 Å to 2.56 Å during Na extraction, and then returns to its original state upon discharge. Importantly, the absence of any new pre-edge feature formation throughout the charge-discharge cycle confirms that no significant distortion in the environment around Fe nor an irreversible migration of Fe. During first charge Mn K-edge energy remains unchanged but shifts to lower energies upon discharging to 2.0 V consistent with the partial reduction of Mn<sup>4+</sup> to Mn<sup>3+</sup>. Mn-O distance decreases to 1.39 Å upon charging and remains unchanged even after subsequent discharging.

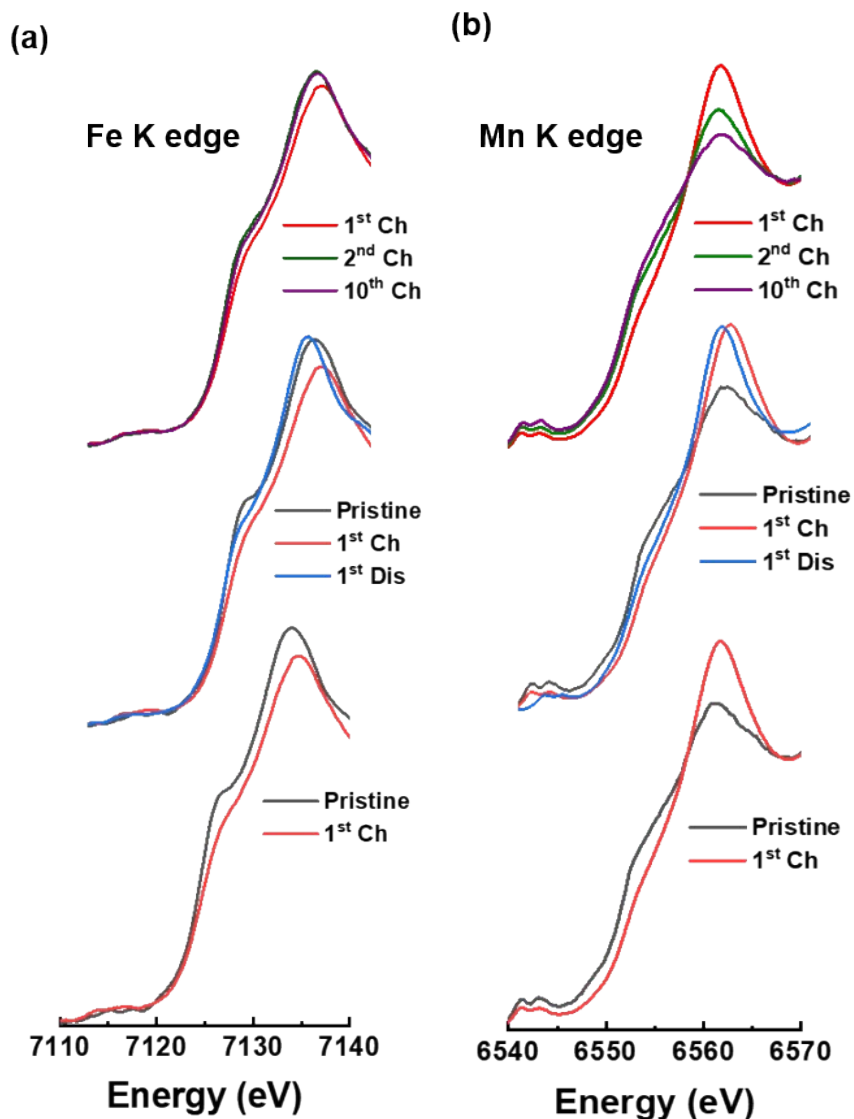


**Figure S13.** Normalized ex situ XANES spectra of (a) Fe and (b) Mn K-edges collected at different states of charge in multiple cycles for NLFM.

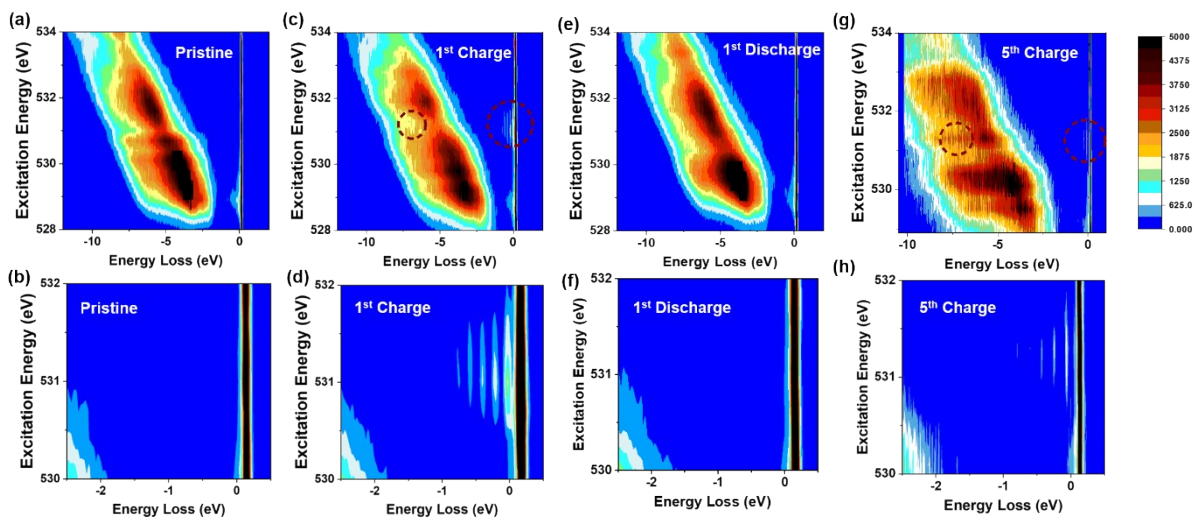


**Figure S14.** High resolution RIXS maps for (a, b) pristine, (c, d) 1<sup>st</sup> charge and (e, f) 1<sup>st</sup> discharge and (g, h) 5<sup>th</sup> charge for checking the molecular O<sub>2</sub> vibrations.

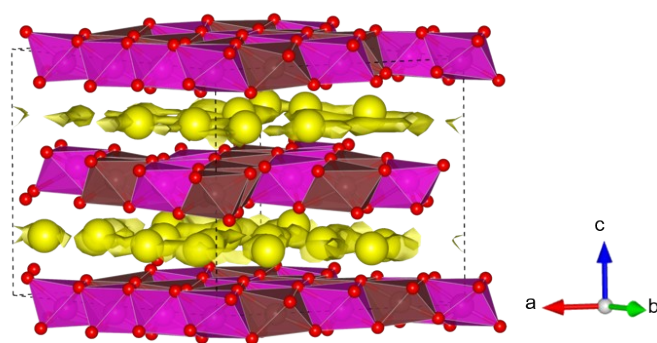


**Figure S15.** Structural illustration in P2- $\text{Na}_x\text{Fe}_{0.5}\text{Mn}_{0.5}\text{O}_2$  for  $x = 0.67$  showing negligible displacement, indicating structural stability.

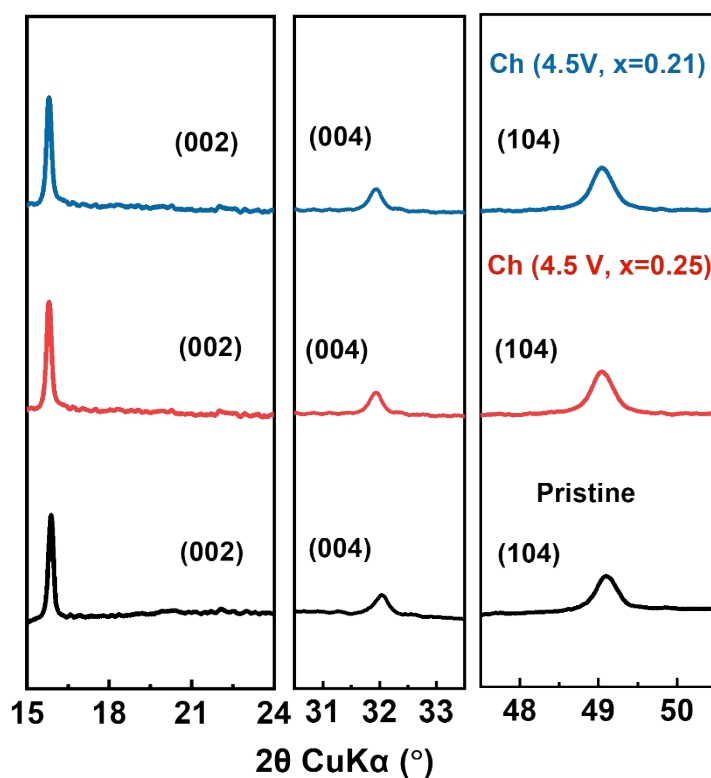


**Figure S16.** Ex situ XRD patterns of NLFM ( $\text{Na}_x\text{Li}_{0.127}\text{Fe}_{0.127}\text{Mn}_{0.746}\text{O}_2$ ) at highest charge state (4.5 V) at C/10 rate ( $x = 0.25$ ) and highly desodiated state ( $x = 0.21$ ).

The P2- $\text{Na}_{0.67}\text{Li}_{0.1}\text{Fe}_{0.37}\text{Mn}_{0.53}\text{O}_2$  cathode, as reported by Wang *et al.*<sup>9</sup>, exhibits substantial O-phase formation when the sodium content is reduced to 0.26. This composition has a lower lithium and higher iron content compared to NLFM. In our study, we typically charged the material up to 4.5 V at a C/10 rate but did not observe any O-type phase transition at  $x = 0.25$ . To further investigate phase transitions in highly desodiated state, we charged the material at a C/10 rate up to 4.2 V, followed by a slower C/25 rate from 4.2 V to 4.5 V. Using this show charging we were able to desodiate NLFM cathode to as low as  $x = 0.21$ . However, even at  $x = 0.21$  moles, we observe continuous left shift of (002) and (004) peaks indicating that the *O-type phase remains absent* in NLFM.

**Table S3.** Relative energy comparison of predicted P2-Na<sub>0.625</sub>Li<sub>0.125</sub>Fe<sub>0.125</sub>Mn<sub>0.75</sub>O<sub>2</sub> (comparable to NLFM) structures with Li atoms positioned in transition metal layers.

Structure No.	Relative Energy meV/atom	Structure No.	Relative Energy meV/atom
S1	0	S15	10.59
S2	22.10	S16	24.99
S3	27.09	S17	13.37
S4	31.18	S18	13.01
S5	11.59	S19	12.10
S6	20.48	S20	15.15
S7	43.41	S21	19.19
S8	17.58	S22	20.01
S9	3.64	S23	10.96
S10	16.33	S24	44.52
S11	26.98	S25	21.90
S12	11.98	S26	13.27
S13	29.77	S27	21.74
S14	24.22	S28	12.64

**Table S4.** Relative energy comparison of predicted P2-Na<sub>0.79</sub>Li<sub>0.210</sub>Fe<sub>0.125</sub>Mn<sub>0.667</sub>O<sub>2</sub> (comparable to NLFM1) structures.

Structure No.	Relative Energy meV/atom	Structure No.	Relative Energy meV/atom
S1	13.08	S15	0
S2	14.37	S16	28.86
S3	16.29	S17	27.78
S4	22.48	S18	26.55
S5	27.40	S19	7.86
S6	7.95	S20	4.65
S7	21.13	S21	13.54
S8	16.23	S22	26.58
S9	11.72	S23	27.64
S10	11.48	S24	10.70
S11	17.50	S25	18.47
S12	18.76	S26	10.80
S13	15.25	S27	19.56
S14	11.33	S28	17.40

**Table S5.** ICP-OES Composition Validation

Theoretical Chemical formula	Measured atomic ratio			
	Na	Li	Fe	Mn
$\text{Na}_{0.702}\text{Li}_{0.127}\text{Fe}_{0.127}\text{Mn}_{0.746}\text{O}_2$ (NLFM)	0.705	0.129	0.131	0.742
$\text{Na}_{0.80}\text{Li}_{0.22}\text{Fe}_{0.14}\text{Mn}_{0.64}\text{O}_2$ (NLFM1)	0.806	0.226	0.142	0.634

**Table S6.** Experimental and theoretical compositions of P2-NLFM and P2-NLFM1

Target Material	Experimental Composition	Theoretical Composition
P2-NLFM	$\text{Na}_{0.702}\text{Li}_{0.127}\text{Fe}_{0.127}\text{Mn}_{0.746}\text{O}_2$	$\text{Na}_{0.625}\text{Li}_{0.125}\text{Fe}_{0.125}\text{Mn}_{0.75}\text{O}_2$
P2-NLFM1	$\text{Na}_{0.80}\text{Li}_{0.22}\text{Fe}_{0.14}\text{Mn}_{0.64}\text{O}_2$	$\text{Na}_{0.79}\text{Li}_{0.210}\text{Fe}_{0.125}\text{Mn}_{0.667}\text{O}_2$

**Table S7.** Profile matched parameters for XRD data of NLFM Pristine, 1<sup>st</sup> charge, 1<sup>st</sup> discharge and 100<sup>th</sup> discharge samples.

Sample	a = b (Å)	c (Å)	Volume (Å <sup>3</sup> )
Pristine	2.901 (7)	11.129 (5)	81.15 (5)
1 <sup>st</sup> Charge	2.870 (8)	11.157 (7)	79.63 (7)
1 <sup>st</sup> Discharge	2.925 (9)	10.959 (2)	81.25 (1)
100 <sup>th</sup> Discharge	2.886 (1)	11.193 (1)	80.74 (7)

**Table S8.** Profile matched parameters for XRD data of NFM Pristine and 1<sup>st</sup> charge samples.

Sample	a = b (Å)	c (Å)	Volume (Å <sup>3</sup> )
Pristine	2.942 (4)	11.231 (1)	84.21 (1)
1 <sup>st</sup> Charge	2.876 (8)	10.272 (4)	73.61 (7)

**Table S9.** Evolution of c-lattice parameter (c-LP) and average Bader charges on O atoms in P2-NLFM from discharged (Na = 0.625) to charged (Na = 0.25) states.

State of Charges (SOCs)	c-Lattice Parameter (Å)	% Volume change	Average Charge on Oxygen
$\text{Na}_{0.625}\text{Li}_{0.125}\text{Fe}_{0.125}\text{Mn}_{0.75}\text{O}_2$	11.25694	0	-1.1438
$\text{Na}_{0.25}\text{Li}_{0.125}\text{Fe}_{0.125}\text{Mn}_{0.75}\text{O}_2$	11.43977	0.913	-1.0092

**Table S10.** Mössbauer spectral parameters of NLFM (pristine) and NLFM (charged, 4.5 V) samples at room temperature where,  $\delta_{IS}$  = isomer shift (relative to Fe metal foil),  $\Delta E_Q$  = quadrupole splitting,  $\Gamma$  = full width at half maximum,  $R_A$  = relative spectral area.

Sample code	$\delta_{IS}$ (mm/s) $\pm 0.002$	$\Delta E_Q$ (mm/s) $\pm 0.005$	$\Gamma$ (mm/s) $\pm 0.01$	$R_A$ (%) $\pm 1$	Fe-Site Doublet	Goodness of fit ( $\chi^2$ )
NLFM (Pristine)	0.343	0.714	0.278	100	Doublet Fe <sup>3+</sup>	1.09
NLFM (Charged, 4.5V)	0.333	0.748	0.349	71.8	Doublet Fe <sup>3+</sup>	1.00
	0.007	0.522	0.589	28.2	Doublet Fe <sup>4+</sup>	

### References

- S1. V. Siruguri, P. D. Babu, M. Gupta, A. V. Pimpale, P. S. Goyal, *Pramana*, 2008, **71**, 1197.
- S2. J. Rodríguez-Carvajal, *Phys. B Condens. Matter*. 1993, **192**, 55.
- S3. P. E. Blöchl, *Phys. Rev. B Condens. Matter*, 1994, **50**, 17953.
- S4. J. P. Perdew, K. Burke, M. Ernzerhof, *Phys. Rev. Lett.* 1996, **77**, 3865.
- S5. G. Kresse, J. Furthmüller, *Phys. Rev. B Condens. Matter*, 1996, **54**, 11169.
- S6. G. Kresse, J. Furthmüller, *Comput. Mater. Sci.* 1996, **6**, 15.
- S7. S. L. Dudarev, G. A. Botton, S. Y. Savrasov, C. J. Humphreys, A. P. Sutton, *Phys. Rev. B Condens. Matter*, 1998, **57**, 1505.
- S8. V. I. Anisimov, J. Zaanen, O. K. Andersen, *Phys. Rev. B Condens. Matter*, 1991, **44**, 943.
- S9. H. J. Monkhorst, J. D. Pack, *Phys. Rev. B*. 1976, **13**, 5188.
- S10. K. Momma, F. Izumi, *J. Appl. Crystallogr.* 2011, **44**, 1272.
- S11. W. G. Hoover, *Phys. Rev. A*. 1985, **31**, 1695.
- S12. Z. Zhu, I.-H. Chu, Z. Deng, S. P. Ong, *Chem. Mater.* 2015, **27**, 8318.
- S13. S. P. Ong, W. D. Richards, A. Jain, G. Hautier, M. Kocher, S. Cholia, D. Gunter, V. L. Chevrier, K. A. Persson, G. Ceder, *Comput. Mater. Sci.* 2013, **68**, 314.
- S14. L. Van Hove, *Phys. Rev.* 1954, **95**, 249.